ACS Catalysis

Research Article

pubs.acs.org/acscatalysis

Theoretical Study of the Free Energy Surface and Kinetics of the Hepatitis C Virus NS3/NS4A Serine Protease Reaction with the NS5A/5B Substrate. Does the Generally Accepted Tetrahedral Intermediate Really Exist?

José Ángel Martínez-González,[†] Miguel González,*[,‡] Laura Masgrau,*[,§] and Rodrigo Martínez*[,†]

[†]Departamento de Química, Universidad de La Rioja, C/Madre de Dios, 51, 26006 Logroño, Spain

[‡]Departament de Química Física i IQTC, Universitat de Barcelona, C/Martí i Franquès, 1, 08028 Barcelona, Spain

[§]Institut de Biotecnologia i de Biomedicina, Universitat Autònoma de Barcelona, 08193 Bellaterra, Barcelona, Spain

Supporting Information

ABSTRACT: The self-consistent charge density functional tight binding/molecular mechanics (SCC-DFTB/MM) and ensemble averaged variational transition state theory/multidimensional tunneling (EA-VTST/MT) methods have been employed to investigate the reaction mechanism and to calculate the rate constant of the NS3/NS4A + NS5A/5B acylation reaction. This reaction belongs to the vital cycle of the hepatitis C virus once it infects the human cell. A concerted reaction mechanism, with a single transition state in which the tetrahedral geometry has already been adopted and the peptide bond is starting to break, has been determined. This reaction supposes an example where the proposed general two-step serine protease acylation reaction mechanism does not occur, being related to the fact that the enzyme is particularly efficient for the NS5A/5B substrate. The transition state characterized here for the acylation reaction can be a good initial structure in the reach of NS3/NS4A inhibitors based on TS analogues. On the other hand, the calculated and experimental phenomenological free energy barriers only differ by 2.3 kcal mol^{-1}, although this leads to a significant discrepancy between calculated and experimental. The rest of the calculated kinetic parameters, such as the kinetic isotopic effect (H/D), tunneling, and the recrossing contributions to reactivity, agree with the expected behavior for the studied reaction.

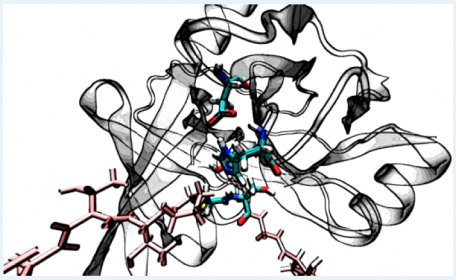

KEYWORDS: *hepatitis C virus, NS3/NS4A serine protease, enzyme catalysis, QM/MM reaction mechanism, rate constant, SCC-DFTB/MM, EA-VTST/MT, concerted mechanism in serine protease reaction*

1. INTRODUCTION

It is estimated that around 130−150 million people are infected by the hepatitis C virus (HCV) worldwide,[1] and this is becoming an important indication for liver transplantation, because near of 27% of all cases of liver cirrhosis and 25% of hepatocellular carcinomas could be related to this infection.[2] Although new drugs have been recently licensed, as simeprevir, and others are in advanced phases of study,[3] unfortunately, there is not a 100% effective medical treatment yet and the main therapeutic approach results from a combination of antivirals with ribavirin and pegylated interferon-α (PEG-INFα), even though the new treatments allow interferon-free therapies for certain HCV genotypes.[3]

The NS3/NS4A protease catalyzes several reactions that occur inside the human cell after infection by HCV, and its inhibition is one of the main strategies to develop new drugs against HCV,[4,5] where computational chemistry has played an important role.[6] This enzyme is produced after proteolytic cleavage by host and viral proteases of a large polyprotein (~3000 amino acids) produced by the human ribosome after translation of the viral mRNA liberated by HCV once endocyted. This cleavage liberates the following viral proteins: C (core protein), E1 and E2 (envelope glycoproteins), p7, NS2, NS3, NS4A, NS4B, NS5A, and NS5B (nonstructural proteins).[4] The NS3 protein (~70 kDa) is a multifunctional protein essential for the virus replication. The 180 amino acids of the N-terminal domain are responsible, together with the cofactor NS4A, for the proteolytic cleavage at the NS3/4A, NS4A/4B, NS4B/5A, and NS5A/5B peptide junctions of the original polyprotein.[4] In the absence of the NS4A polypeptide cofactor, the NS3 protease folds in two structural subdomains, the N- and C-terminal domains.

As in other proteins of the chymotrypsin family with the same relative spatial positions,[7] the active site of NS3 is formed by the His-Asp-Ser catalytic triad and the oxyanion stabilizing group (residues 135−139), whereas the βE2 strand is found in the specificity pocket. The His-57 and Asp-81 residues belong to the N-terminal subdomain, and the Ser-139 residue belongs

Received: August 1, 2014
Revised: November 20, 2014
Published: December 5, 2014

Scheme 1. Generally Proposed Reaction Mechanism for the Acylation Process Catalyzed by the NS3/NS4A Protease

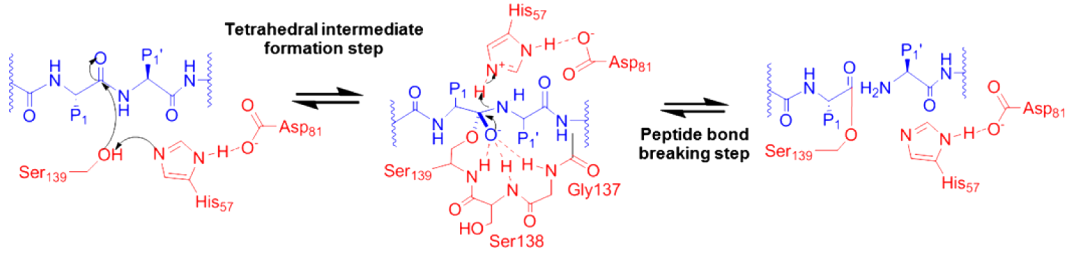

to the C-terminal subdomain.[8] The binding of NS4A to NS3 rearranges the NS3 active site toward the optimal geometrical configuration for catalysis.[9] Given their structural similarities and the fact that NS3/NS4A and chymotrypsin have similar inhibitors,[8] it has been proposed that both enzymes present a similar reaction mechanism.[10,11] Thus, once the Michaelis complex is formed, the imidazole ring of His-57 is positioned to be able to deprotonate the nucleophilic −OH group of Ser-139, and the side chain of Asp-81 is oriented to stabilize the resulting positive charge created in His-57. The acylation process would start with the nucleophilic attack of the carbonyl C atom by the −OH group of Ser-139, leading to a tetrahedral intermediate that can be stabilized by hydrogen bonds with some residues of the oxyanion stabilizing loop (residues 135−139).[7] NMR studies of the NS3/NS4A structure covalently bonded to an inhibitor[9] found hydrogen bonds in the tetrahedral structure between the hemiketal oxygen and the amide groups of Ser-139 and Gly-137. They also suggest that Arg-155 contributes to the catalysis by shielding, through its side chain, the interaction between His-57 and Asp-81 from the solvent,[12] reinforcing the hydrogen bond between them. Lys-136 from the oxyanion loop and Arg-109 seem to be involved in the recognition of the substrate and were used as starting points in the development of inhibitors.[13,14]

Then, the peptide bond would break, releasing the N-terminus of the peptide substrate and acylenzyme. In the deacylation step, this species is hydrolyzed by a water molecule and the C-terminus of the substrate and the enzyme are liberated.[11] On the other hand, several crystal structures of the NS3 protease show a zinc binding site, where the Zn^{2+} presents a tetrahedral coordination bonded to Cys-97, Cys-99, Cys-145, and a water molecule (which at the same time is hydrogen bonded to His-149). However, this cation is remotely located from the active site; thus, a structural rather than catalytic role is supposed for the Zn^{2+}.[7]

Several kinetic studies based on alanine scanning and HCV RNA mutation experiments with different substrates and inhibitors have been performed.[15−24] However, in the context of this contribution, among these studies it is important to note the measurement of NS3/NS4A enzyme kinetic data for the cleavage of three synthetic substrates that mimic the natural substrates:[16] NS5A/5B, NS4B/5A, and NS4A/4B.

Serine proteases have been extensively studied,[11] and various quantum mechanics/molecular mechanics (QM/MM) studies can be found.[25−30] Regarding the NS3/NS4A enzyme, our group has applied the QM/MM hybrid approach to describe the reaction mechanism with its three natural substrates and the effect of enzyme mutations on it.[12,31−33] In these works, technical details of the calculations, such as the size of the zone where the quantum method is applied, the boundary treatment between QM-MM zones, and the effect of different quantum levels on the potential energy surfaces of the reactions, have been characterized for this enzyme.

In general terms, these studies agree[31−33] with the reaction mechanism proposed for chymotrypsin, showing that of the two processes (acylation and deacylation) the rate-limiting step is the acylation process, whose rate would in turn be determined by formation of a stable tetrahedral intermediate. However, the calculated barriers[12] are much larger than the experimental[16] ones, although they are reduced when ab initio quantum methods are used to improve the initial results.[12] Interestingly, in a recent study of the NS3/NS4A protease with the three different substrates,[33] it has been shown that the correction of the AM1/MM free energy with higher level (MP2; second-order Møller−Plesset method) energies and an increase of the basis set used for the QM calculations diminish the stability of the tetrahedral intermediate and the height of the acylation barrier. The results pointed out the possibility that for reaction with the NS5A/5B substrate, despite keeping acylation as the overall rate-limiting process, a stable tetrahedral intermediate species could not exist; the acylation step would then be a concerted process with a single late transition state, in which the peptide bond is already breaking.

In this work we have employed a QM/MM approach to characterize the reaction mechanism and calculate for the first time the rate constant of the enzymatic reaction involving the NS3/NS4A protease and the NS5A/5B substrate, continuing the in-depth study of this reaction and related systems performed by our group. In particular, we have used the QM(SCC-DFTB; self-consistent charge density functional tight binding)/MM molecular dynamics method[34] to calculate the free energy changes associated with the two chemical steps of the reaction. Moreover, we have introduced quantum corrections to the free energies[35] by means of the ensemble averaged variational transition state (EA-VTST) methodology,[36−38] which also includes an estimation of multidimensional tunneling (MT) and recrossing effects, in order to get a better description of the free energy of the intermediates and transition states that may occur in the reaction.

In section 2 the computational tools and calculation details are exposed. In section 3 the most valuable results are shown, whereas a summary and the conclusions of the work are given in section 4.

2. COMPUTATIONAL METHODS

2.1. Initial Structure, QM/MM Level, and QM-MM Partition. The initial structure used in this study has been employed by our research group in previous works.[12,31−35] It corresponds to a NS3/NS4 + NS5A/5B complex solvated with a sphere of radius 37 Å of TIP3P water molecules, which has been shown to be stable in various classical and QM/MM (with the semiempirical AM1 as the quantum method) simulations.

dx.doi.org/10.1021/cs5011162 | ACS Catal. 2015, 5, 246−255

This structure was built from an experimental X-ray apo structure (PDB code 1DXP) selected on the basis that was the best suited to deprotonate Ser-139 (closest Ser-139-Os His-57-Nε distance in the structure), which is a central issue in the proposed reaction mechanism. The structure was subsequently modified to mimic the NS3/NS4A + NS5A/5B complex (see refs 12 and 31 for further information).

The SCC-DFTB method[39,40] has been used as the quantum level to describe the atoms included in the QM region. The rest of the enzyme and substrate and the water molecules that solvate the system have been described by the CHARMM22[41] force field. Therefore, the SCC-DFTB/CHARMM22 method[34] has been applied using the CHARMM program (version c35b1)[42] and following an additive scheme in the calculation of the interaction Hamiltonian.[43] The SCC-DFTB method is computationally efficient and has demonstrated its usefulness in the study of biological systems (see e.g. refs 44 and 45 and references therein).

The reactive process has been studied by considering the two elementary steps involved in the acylation process, following the proposed general mechanism, shown in Scheme 1: nucleophilic attack (or tetrahedral intermediate formation step) and breaking of the peptide bond. Note that the last process (acylenzyme hydrolysis or deacylation process) has not been considered in this study; thus, when the products are cited, they are referenced to the acylenzyme and the N-terminal part of the lysed substrate.

In all, 57 atoms define the part of the system included in the quantum region of the QM/MM calculations. These atoms, represented in Scheme 2, are part of the NS3 catalytic triad

Scheme 2. Fragment of the NS5A/5B Substrate and Residues (Catalytic Triad) of the NS3 Protease Included in the QM Region[a]

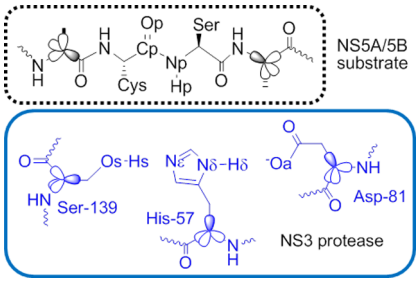

[a]The GHO frontier atoms are also indicated (sp^3 orbitals).

(His-57, Asp-81, and Ser-139) as well as the substrate amino acids which are closer to the scissile bond. The rest of the atoms, a total of 11015, form the MM part of the system. The generalized hybrid orbital (GHO) approach[46,47] has been used to account for the five bonds that cross the QM/MM boundary, which are also shown in Scheme 2. Both the partition scheme and boundary method are suitable for this and related systems, as was shown in ref 32.

The electrostatic and van der Waals nonbonded interactions were switched and shifted to 0, respectively, in the range 12.0–13.5 Å. The relative dielectric constant for the MM electrostatic interactions was $\varepsilon = 1$.

2.2. Energy Minimization, Grid Setup, and Potential of Mean Force. From the enzyme–substrate–water structure described before, the QM/MM potential energy was minimized using the adapted basis Newton–Raphson (ABNR) method[48] until the root-mean-square deviation of the gradient (GRMS) was lower than 0.0001 kcal mol^{-1} Å^{-1}. This model of the Michaelis complex of the enzymatic reaction was used as the initial point for the study of the potential of mean force and the region of the free energy surface of the Ser-139 nucleophilic attack.

Three distinguished reaction coordinates (χ in a general form) have been defined to describe this process (see Scheme 2 for atom naming): (1) the Os–Cp distance, i.e. the nucleophilic attack of oxygen of Ser-139 to the substrate's carbonylic carbon; (2) the difference between the Os–Hs and Hs–Nε distances, representing the Hs proton transfer between the Ser-139 oxygen and the His-57 ε nitrogen; (3) the antisymmetric combination of the two previous processes.

To describe the products of the nucleophilic attack, the relevant interatomic distances of the system were artificially modified to reproduce an approximate product geometry. After this, the QM/MM potential energy was minimized (ABNR method, GRMS < 0.0001 kcal mol^{-1} Å^{-1}), giving an optimized structure that corresponds to a tetrahedral intermediate, which was considered as the starting point of the peptide bond breakage process study. This step has been investigated through the following reaction coordinates: (1) the breaking Cp–Np distance; (2) the difference between the Np–Hs and Nε–Hs distances, describing the proton transfer from the nitrogen of the His-57 to the nitrogen of the substrate; (3) the antisymmetric combination of (1) and (2). As can be seen in refs 12–31, the selected set of coordinates is suitable for describing the studied processes.

The classical potential of mean force (PMF or $W_{CM}(T,\chi)$ henceforth) and the corresponding part of the classical free energy surface (FES) of both reaction steps have been calculated including temperature effects on the system simulation. Note that the CM (classical mechanical) subindex is used to indicate that, despite the fact that the description of the potential energy is done at the QM/MM level, the nuclei move (dynamics) according to Newton's equations of motion. The stochastic boundary molecular dynamics (SBMD) method[49] has been employed to heat the Michaelis complex and product structures to 300 K, assigning the velocities from a Maxwell distribution during 100 ps of molecular dynamics (MD) simulation. They were subsequently equilibrated over 500 ps, using a buffer region of 26 Å, an integration time step of 1 fs, and the SHAKE algorithm[50] to constrain the nonquantum H–X bonds. The van der Waals and electrostatic nonbonded interactions were considered as described above.

Starting from the equilibrated Michaelis complex and putative tetrahedral intermediate structures, for the nucleophilic attack and peptide bond breaking processes, respectively, the umbrella sampling (US) technique[51] was applied to the subsequent combination of discrete coordinates. An umbrella potential of V = 50 kcal mol^{-1} Å^{-2} $\Delta\chi^2$ was applied at every 0.1 Å along each coordinate. At every considered point, 15 ps of equilibration simulation was calculated, followed by 50 ps of production simulation (only these last simulation results are included in the analysis), using the conditions described above.

Using the US simulations the reaction is driven from reactants to products by the umbrella potential. Hence, to extract the real thermodynamic information from these results it is necessary to eliminate the effect of this driving force and to apply the corresponding statistical thermodynamics equations to evaluate the change of free energy involved in the process. This was done by means of the WHAM (weighted histogram

dx.doi.org/10.1021/cs5011162 | ACS Catal. 2015, 5, 246–255

analysis method)[52,53] analysis, which can be applied to one- or two-dimensional US simulations, depending on whether the PMF (or free energy profile) or the FES is going to be calculated.

2.3. EA-VTST/MT Method. The ensemble averaged variational transition state/multidimensional tunneling method[36−38] is a procedure that has been developed for including quantum vibrational energies, nuclear tunneling, and recrossing in the theoretical study of enzyme kinetics. Within this framework, the variational transition state theory rate constant ($k^{CVT}(T)$) is calculated as

$$k^{CVT}(T) = \gamma(T)\frac{k_B T}{h}\exp\left(-\frac{\Delta G^{\ddagger}_{QC}}{RT}\right) \quad (1)$$

where k_B, h, R, and T are the Boltzmann, Planck, and ideal gas constants and temperature, respectively. $\Delta G^{\ddagger}_{QC}$ is the quasiclassical (QC) free energy of activation (see below), and $\gamma(T)$ is the overall transmission coefficient that considers the dynamical corrections by including two effects:

$$\gamma(T) = \Gamma(T)\kappa(T) \quad (2)$$

Thus, the recrossing transmission coefficient, $\Gamma(T)$, corrects the rate constant for trajectories that recross the classical transition state dividing hypersurface back to the reactant asymptote. It lies between 0 and 1, with values less than unity arising from the coupling of the reaction coordinate to other coordinates.[54] The $\kappa(T)$ coefficient accounts for quantum tunneling and is, in general, equal to or greater than 1.

In order for a comparison with experimental kinetic data, the phenomenological activation free energy ($\Delta G^{\ddagger}_{phen}(T)$) is defined as

$$\Delta G^{\ddagger}_{phen}(T) = -RT\ln(\gamma(T)) + \Delta G^{\ddagger}_{QC}(T) = \Delta G^{\ddagger}_{\gamma}(T) + \Delta G^{\ddagger}_{QC}(T) \quad (3)$$

which can be conveniently compared with the experimental phenomenological activation free energy (ΔG^{exp}_{phen}) obtained by applying eq 4 (classical Eyring equation) to analyze the experimental rate constant values:

$$k^{exp}(T) = \frac{k_B T}{h}\exp\left[-\frac{\Delta G^{exp}_{phen}(T)}{RT}\right] \quad (4)$$

The application of the EA-VTST/MT method is carried out in three steps. The first involves the calculation of the PMF. The estimated classical activation free energy, $W_{CM}(T,\chi)$, is then corrected in step 2 to include the quantization of the vibrational modes (except that corresponding to the distinguished reaction coordinate). To do so, instantaneous generalized normal-mode analysis[35] is performed for a subsystem of atoms (typically, but not necessarily, all atoms in the QM region), considering several configurations sampled from the umbrella sampling simulations. The frequencies obtained are used to calculate the difference between the quantum and classical vibrational energies (ΔW_{vib}), which is added to the classical PMF along the reaction coordinate[35] to obtain the quasi-classical potential of mean force ($W_{QC}(T,\chi)$), from which tunneling and recrossing are still excluded. From this quasiclassical PMF, the quasiclassical activation free energy ($\Delta G^{\ddagger}_{QC}(T)$) included in eq 1 is calculated as

$$\Delta G^{\ddagger}_{QC}(T) = W_{QC}(T,\chi^{\ddagger}) - [W_{QC}(T,\chi^{R}) + G_{F,QC}(T)] + \Delta C(\chi) \quad (5)$$

where $\chi^{\ddagger}$ and χ^{R} denote the reaction coordinate values at the transition state (the maximum of the $W_{QC}(T,\chi)$ profile) and the reactant state, respectively, $G_{F,QC}$ is the quantum mechanical vibrational free energy of the reactant state corresponding to mode F, which is that which correlates with the distinguished reaction coordinate, and $\Delta C(\chi)$ is a Jacobian correction (usually neglected) resulting from the use of a non-Cartesian reaction coordinate.

In the present work, 100 structures for each umbrella simulation window (a total of 6700 structures) were used in this second step. For every structure, normal mode analysis was carried out for the atom selection shown in Figure S1 of the Supporting Information. This atom selection for the vibrational calculation is smaller than the initial QM zone, because it was impossible to converge the calculations of the vibrational frequencies using a larger definition. Finally, the vibrational correction factor, ΔW_{vib}, was calculated as an average in each χ value.

The third step in the EA-VTST/MT scheme involves the calculation of the transmission coefficient, which actually is an average over different reaction paths where individual Γ_i and κ_i factors are calculated. A certain number of structures (25 in this work) were taken from the umbrella sampling simulation at the value of χ where the maximum of $\Delta G^{\ddagger}_{QC}(T)$ is located. For every selected structure, the minimum energy path (MEP) is determined for the QM selection, whereas the MM part of the system is frozen. The computation of Γ_i and κ_i values is carried out on the effective potential of a different static MM configuration.[36,37] The recrossing factors were calculated following an approximation to the dynamic recrossing transmission coefficient,[55] whereas the tunneling was evaluated by the optimized multidimensional tunneling (OMT) approximation.[56] With all this, $k^{CVT}(T)$ and $\Delta G^{\ddagger}_{phen}(T)$ can be calculated using eqs 1 and 3.

Steps 2 and 3 were carried out for the reaction of the NS3/NS4A protease with the NS5A/5B substrate and the deuterium isotopic substitution shown in Figure S1 (deuterated hydroxyl of Ser-139). Thus, the rate constants for both the H and D isotopes have been calculated and the corresponding kinetic isotope effect (KIE) has been predicted.

The application of these second and third steps was carried out using the CHARMMRATE[57] program, which is an interface between the CHARMM[42] and POLYRATE[58] programs.

3. RESULTS AND DISCUSSION

3.1. SCC-DFTB/MM Classical Free Energy Results. Previous to the free energy calculations, explorations of the potential energy surface (PES) and minimum energy paths were performed. These results, which include the structural and energetic information on the singular points found on the PES, are given in the Supporting Information (Figures S3−S6 and Table S2).

To describe the reaction mechanism of the acylation process catalyzed by the NS3/NS4A serine protease, the free energy profiles of both the formation of the tetrahedral intermediate and the peptide bond breaking processes were calculated by varying the combination of the interatomic distances and using the calculation setup described previously. Thus, the classical

dx.doi.org/10.1021/cs5011162 | ACS Catal. 2015, 5, 246−255

PMF (or classical free energy profile) at 300 K was calculated for the two processes by applying the US simulation technique, following the discrete coordinates described in section 2.2. The results of these calculations are depicted in Figure 1.

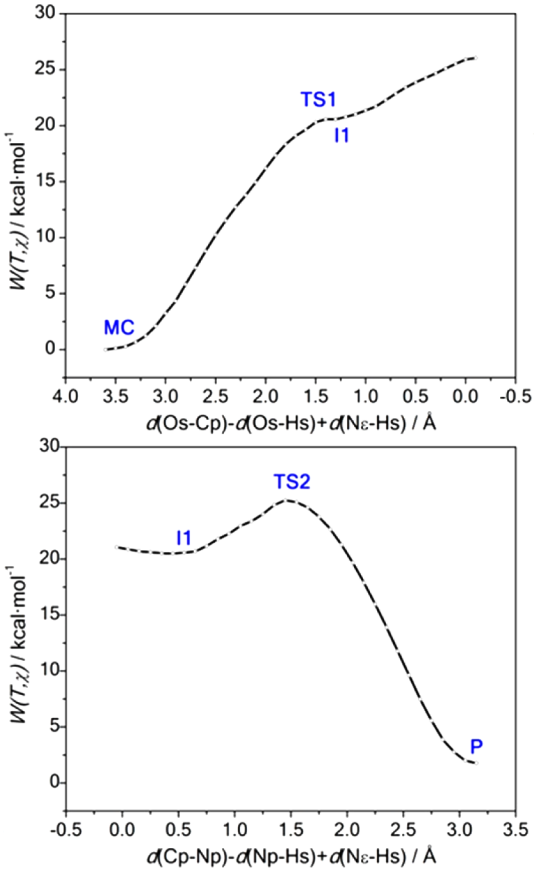

Figure 1. SCC-DFTB/MM classical free energy profiles (or PMF) for the tetrahedral intermediate formation (top) and peptide bond breakage (bottom) for the reaction of the NS3/NS4A protease with the NS5A/5B substrate. The zero of energy is taken at the MC point (Michaelis complex).

In the classical PMF results there is a free energy barrier (TS1, 20.6 kcal mol^{-1} relative to the Michaelis complex; Table 1) and an energetic plateau that could be interpreted as an intermediate (I1), although the energy difference between the barrier and the intermediate is so small (only 0.1 kcal mol^{-1}, see Table 1) that its lifetime would be too short to actually be considered as such.

Table 1. Classical Free Energies of the Stationary Points Referenced to the Michaelis Complex (MC)

	ΔG_{CM}/kcal mol^{-1}
MC	0.0
TS1	20.6
I1	20.5
TS2	25.2
P	1.8

This I1 structure further evolves through a barrier, TS2, into the acylation products. The classical free energy for this barrier is 25.2 kcal mol^{-1} relative to the Michaelis complex and is located at the reaction coordinate value χ = 1.5 Å. The free energy difference between I1 and TS2 is 4.7 kcal mol^{-1}.

Note that the classical free energy barrier for the TS2 point (25.2 kcal mol^{-1}) seems too high for an enzymatic process and overestimates the experimental phenomenological activation free energy for the present reaction (ΔG^{exp}_{phen} = 18.7 kcal mol^{-1}, derived from a experimental rate constant of 6.25 min^{-1} at 296 K and application of eq 4).[16] This is probably due to the error associated with the description of the QM/MM potential and also to the fact that vibrational modes are still not quantized at this point.

Figure 2 presents the three-dimensional representations of the classical free energy surface regions for both steps, where all of the intermediates and barriers described above can be seen. On the equipotential contour plot representations (right panels in Figure 2), a selection of the points sampled during the umbrella sampling simulations that produced the classical free energy profiles depicted in Figure 1 are indicated.

3.2. SCC-DFTB/MM Quantum-Corrected Free Energy Results. Once the PMF was calculated and an estimation of the variation of the classical free energy along the reaction (W_{CM}) was obtained, the next step was to carry out the instantaneous normal mode calculations, in order to calculate the difference between the classical and quantum vibrational free energies along the selected reactive coordinates (ΔW_{vib}). This procedure was carried out by considering the H and D (Ser-139) isotopic variants exposed in Figure S1 of the Supporting Information, with the intention of studying the corresponding KIE. The results of this vibrational correction, ΔW_{vib}, for both isotopic systems and reactive steps and the fit of the points using a fifth-degree polynomial function are shown in Figure S2 of the Supporting Information (see the polynomial coefficients in Table S1).

These quantum-corrected (quasiclassical) free energy profiles are shown in Figure 3. Here, the classical PMF results have been also included for comparison purposes. The quantization of the vibrational energy leads to a general decrease of the free energy in both processes and isotopic species. It is important to note that in the tetrahedral intermediate formation profile this decrease causes the complete vanishing of the barrier in both the proton and deuteron transfers and that no quasi-classical free energy minimum is associated with the tetrahedral complex structure. Several energy minimizations were performed by starting from structures taken from the corresponding ensemble labeled as I1 on the PMF profile, and all structures culminated in the Michaelis complex geometries. This suggests that the system could evolve from the Michaelis complex to the TS2 free energy maximum (the only free energy maximum found), crossing a relatively flat zone around the I1 structure, following a concerted acylation step. The vibrational correction also reduces the free energy of TS2, both with respect to the Michaelis complex and with respect to the I1 point. This decrement is somewhat greater in the H^+ transfer process, meaning that this process is slightly faster than the D^+ transfer process, as it usually is. The calculated quasi-classical free energy barriers are $\Delta G^{\ddagger}_{QC}$ = 20.5 and 21.0 kcal mol^{-1} for H^+ and D^+, respectively (Table 2), in better agreement with the experimental value of $\Delta G^{exp}_{phen}(H)$ = 18.7 kcal mol^{-1} in comparison to values determined by the classical methods.

Finally, the transmission coefficient for tunneling and recrossing for this reaction were calculated at 300 K. Thus, following the methodology developed by Truhlar and co-workers,[36−38] several structures from the quasi-classical free

dx.doi.org/10.1021/cs5011162 | ACS Catal. 2015, 5, 246−255

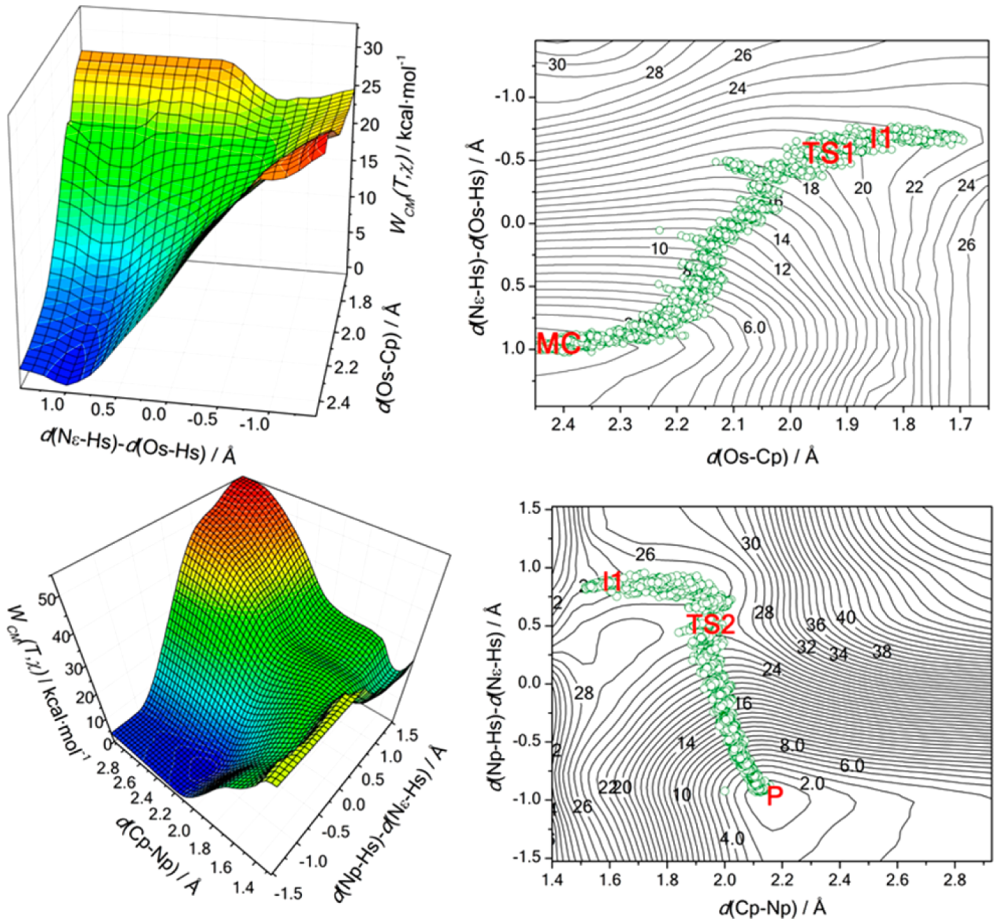

Figure 2. SCC-DFTB/MM classical free energy surface regions for the tetrahedral intermediate formation (top) and peptide bond breaking (bottom) steps for the reaction of the NS3/NS4A protease with the NS5A/5B substrate. Some system structures over the minimum classical free energy path are represented by green circles in the contour plot representations (right).

energy maximum (TS2) were selected and the corresponding minimum energy pathways for the QM zone embedded in the rest of the system were calculated. A total of 25 MEPs for each isotope considered were calculated. Notably, and in agreement with the results shown in the previous sections, all of the minimum energy paths lead directly to the Michaelis complex or to the acylenzyme products. The tunneling (κ) and recrossing (Γ) factors were calculated as a mean of the 25 values obtained. The results of these calculations are exposed in Table 2.

The tunneling transmission coefficients are similar for both isotopes, being somewhat larger in the case of the proton transfer ($\kappa(H^+)$ = 1.19 ± 0.09 vs $\kappa(D^+)$ = 1.14 ± 0.05). Both of them are close to unity, as expected for this reaction, meaning that, although a light atom is transferred in the process, the motion of the several heavy atoms also involved makes the tunneling not very significant here. Thus, the contribution of tunneling would produce a decrement of 0.1/0.1 kcal mol^{-1} on the phenomenological (D^+/H^+) free energy barrier (eq 3), which represents an increase of the rate constant values by ∼14/19%.

The recrossing factors are 0.38 ± 0.22 and 0.47 ± 0.19 in the case of the light and heavy isotope transfers, respectively, which would represent an increase of 0.6/0.5 kcal mol^{-1} (H^+/D^+) in the phenomenological free energy barrier (at T = 300 K). Their values are lower than unity and are in the range of recrossing factors obtained for other enzymatic reactions, although in the lower values, probably reflecting the concerted nature of the real reaction coordinate and the coupling of the environmental degrees of freedom to it.[37] Note that the high values of the standard deviations of the recrossing coefficients are not indicative of an error in the simulations but are a measure of the fluctuations in the physical system for the configurations in a canonical ensemble of transition states.[59] Therefore, they are a reflection of the multiple pathways through which the reaction occurs, since the reactive center is surrounded by a changing environment due to the motion of the rest of the protein and solvent. When both tunneling and recrossing factors are combined, overall transmission coefficients of 0.45 ± 0.26 and 0.53 ± 0.24 are obtained for H and D transfer, respectively, which translate into increments of the free energy barrier by 0.5 and 0.4 kcal mol^{-1}, respectively.

The final (phenomenological) activation free energy, $\Delta G^{\ddagger}_{phen}(T)$, calculated for the acylation reaction of the NS3/NS4A protease with its natural substrate NS5A/5B, is then 21.0 kcal mol^{-1} (eq 3), which is in qualitative good agreement with the experimentally derived phenomenological activation free energy (ΔG^{exp}_{phen} = 18.7 kcal mol^{-1}).[16] Note that the theoretical result still slightly overestimates the experimental value, but the difference (2.3 kcal mol^{-1}) is not far from the error associated with the methods (e.g., the QM/MM potential) and the quantitative insight of 1−2 kcal mol^{-1} reported in ref 60. When the heavier isotope is transferred among Ser-139, His-57, and the leaving fragment, the calculated phenomenological free

dx.doi.org/10.1021/cs5011162 | ACS Catal. 2015, 5, 246−255

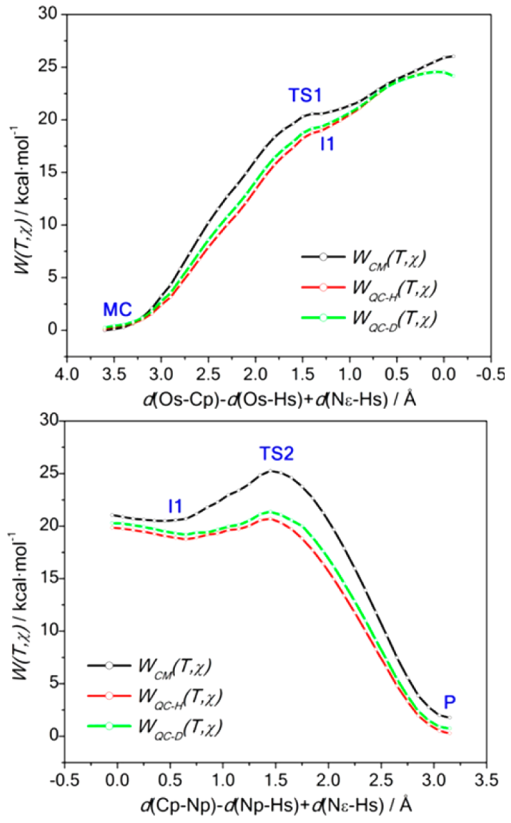

Figure 3. Quantum-corrected (quasi-classical, see section 2.3) SCC-DFTB/MM free energy profiles for the proposed tetrahedral intermediate formation (top) and peptide bond breaking (bottom) steps for the reaction of the NS3/NS4A protease with the NS5A/5B substrate. Proton transfer is represented by red lines, while deuteron transfer is represented by green lines. The classical free energy profiles (Figure 1) have also been included here using black lines. Note that the quasi-classical profiles merge in an essentially concerted acylation step.

Table 2. Kinetic Parameters of the NS3/NS4A + NS5A/5B Acylation Reaction

	proton	deuteron	exp[16]
$\langle\kappa\rangle$	1.19 ± 0.09	1.14 ± 0.05	
$\langle\Gamma\rangle$	0.38 ± 0.22	0.47 ± 0.19	
$\langle\kappa\rangle\langle\Gamma\rangle$	0.45 ± 0.26	0.53 ± 0.24	
$\Delta G^{\ddagger}_{QC}$/kcal mol^{-1}	20.5	21.0	
$\Delta G^{\ddagger}_{phen}$/kcal mol^{-1}	21.0	21.4	18.7[a]
k/min^{-1}	0.20	0.10	6.25
$k^{CVT}(H^+)/k^{CVT}(D^+)$	2.0		

[a]Derived from the experimental k_{cat} value of 6.25 min^{-1} for H^+ (T = 296 K employing a synthetic substrate that mimics the NS5A/5B substrate). Estimated experimental error of 10−30%. Theoretical data at 300 K.

energy barrier is 21.4 kcal mol^{-1}. These values are reported in Table 2 together with the corresponding rate constants and KIEs. It can be seen that the relatively small differences in phenomenological activation free energies between theory and experiment result in larger differences in the rate constants due to the exponential dependence. Thus, the rate constant value for the main process (proton transfer) presents a value of k^{CVT}(300 K) = 0.20 min^{-1} (k^{exp}(296 K) = 6.25 min^{-1}, although the experimental substrate is not exactly the same as the natural species),[16] whereas the value for the isotopic substitution reaction is $k^{CVT}(D^+,300\ K)$ = 0.10 min^{-1}. Hence, the predicted calculated KIE is 2.0, indicating that the reaction involving the proton transfer is twice as fast as the deuteron transfer.

3.3. Implications for the Serine Protease Mechanism.

Now that the exposed data and results have been examined, it is time to think about a proposal for the rate-limiting step of the whole process and, in a more general way, the reaction mechanism.

In the previous AM1/MM studies on the NS3/NS4A enzyme[12,31] the tetrahedral intermediate was clearly found in the three reactions involving the natural substrates (NS5A/5B, subs1; NS5B/4A, subs2; NS4A/4B, subs3); thus, the rate-limiting step was marked as the tetrahedral intermediate formation, this step being analyzed to assess the kinetic agreement with experiments. However, the AM1 quantum method has its limitations, as was shown when the MP2/6-31G* ab initio level was employed to correct and go beyond the AM1/MM results.[12,33]

Experimentally, the detection of the intermediate has been a difficult task and has only been possible under very special experimental conditions (see e.g. ref 61) and with unnatural substrate analogues (e.g. ref 62) or inhibitors (e.g. ref 63). The tetrahedral intermediate has a very short lifetime, which has been proposed to decrease even more as the leaving group improves, becoming a concerted reaction when the lifetime of the intermediate becomes less than the time of a vibration,[11] evidencing a very efficient substrate.

In this work, the calculated classical PMF for the nucleophilic attack shows a small barrier and a very shallow minimum (only 0.1 kcal mol^{-1} difference), but the corresponding barrier for its formation disappears when the vibrational modes of the QM zone are quantized and, thus, a better theoretical estimate of the free energy profile is obtained. Therefore, the Michaelis complex and products turn out to be connected by a unique free energy barrier, without any stable or metastable intermediate between them, although with a flat zone before the transition state. This correlates with a reaction mechanism for the rate-limiting NS3/NS4A + NS5A/5B acylation step that is essentially concerted, with no formation of a stable tetrahedral intermediate (Figure 4).

In a detailed way, the reaction starts with a nucleophilic attack of the oxygen atom of Ser-139 to the carbon atom of the scissile bond. The oxygen atom is activated by proton transfer to the epsilon nitrogen atom of His-57; this transfer creates a positive charge on the histidine's ring that is stabilized through an interaction among the δ nitrogen, the hydrogen bonded to it, and an oxygen atom of the Asp-81 residue. There is no evidence of a complete proton transfer between the nitrogen and oxygen atoms. The oxygen nucleophilic attack and the proton transfer occur simultaneously. The process continues until the peptide bond starts breaking (1.59 Å), at which point the only free energy maximum that is found along the whole process occurs, defining the location of the acylation transition state (see Figure 4 for structural details). From here on, the free energy decreases and the peptide bond gets an even larger separation as the nitrogen of this bond takes the aforementioned hydrogen from the His-57, creating the amino termination of one of the new fragments and the acylenzyme.

Thus, the reaction mechanism of serine proteases in general and NS3/NS4A in particular seems to be more complicated to fit in the generally accepted reaction mechanism. This situation is not exclusive of serine proteases. Thus, in theoretical studies

dx.doi.org/10.1021/cs5011162 | ACS Catal. 2015, 5, 246−255

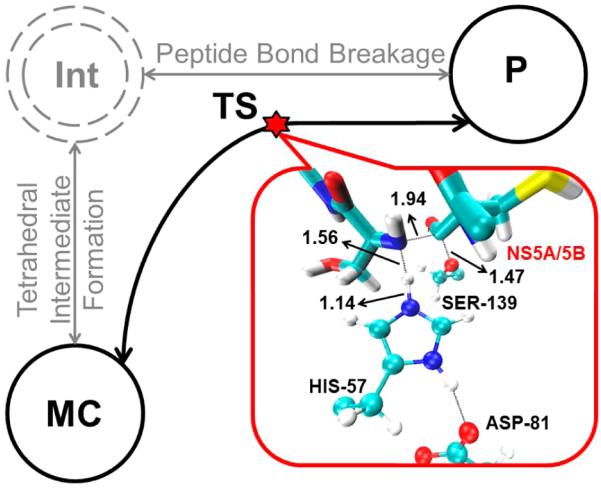

Figure 4. Schematic representation of the concerted acylation mechanism found for the NS3/NS4A protease + NS5A/5B substrate system in front of the generally proposed two-step mechanism. A molecular representation of the transition state characterized is shown, with some average distances indicated.

of *Pseudozyma antartica*[64] and *Candida antartica*[60] lipases, stable intermediate formation (corresponding to the acylenzyme) has been described, but with such a short lifetime that the stepwise and concerted mechanisms would have similar barriers.

Reaction mechanisms have been widely considered in the organic physical chemistry field.[65] Thus, the acylation step in serine protease reactions would fit a preassociation stepwise or preassociation concerted reaction mechanism depending on the lifetime of the tetrahedral intermediate. Thus, when its lifetime is shorter than a vibrational period ($\sim 10^{-13}$ s) the process occurs in a concerted way. In the process studied here, the inclusion of zero-point energies in the calculation of the free energy makes such an intermediate disappear, although the system adopts geometries similar to those expected for the tetrahedral intermediate along the acylation reaction. Going further, the acylation step studied here could be described as an uncoupled concerted reaction,[65] since the concerted reaction involves two processes (nucleophilic attack and bond rupture) but there is no barrier for the collapse of the intermediate and no stable intermediate.

The theoretical characterization of the reaction mechanism made here could be useful in the design of new inhibitors based on transition state analogues,[66,67] as an alternative way of serine traps inhibitors that produce an irreversible compound that mimics the tetrahedral intermediate (see e.g. the PDB entries[68] 1DY8 and 1DY9 or ref 69 for a review of NS3/NS4A covalent inhibitors). Note that the TS2 structure still conserves many features of the tetrahedral intermediate but with a longer C_P–N_P distance and the H_S proton starting to migrate from His57 toward N_P (Figure 2 and Figures S4 and S5, Supporting Information).

The enzyme will present a great affinity for a compound that resembles the geometry and charge distribution of the substrate at the transition state geometry, hopefully in this case greater than the affinity for the natural substrate. In enzymatic reactions there is not a unique transition state structure; they form an ensemble of structures that connect different reactive paths under the influence of the enzyme and solvent environment. Thus, QM/MM molecular dynamics simulations performed here and the identification of the TS2 point as the transition state in the studied reaction could give a good starting point in the analogue search.

4. CONCLUSIONS

The QM/MM method has been applied to elucidate the reaction mechanism of the acylation process of the NS3/NS4A + NS5A/5B proteolysis reaction. This reaction is involved in the HCV replication process; thus, its understanding is important in the fight against one of the most widespread illnesses in the world.

Previous AM1/MM studies about this and related systems[12,31,32] have been used as a starting point to define several features of the calculations such as the definition of the QM part, the use of GHO as a boundary method, the selection of the reaction coordinates, and the optimal calculation numerical parameters. These studies suggested that the reaction follows the generally proposed reaction mechanism for serine proteases: i.e., the tetrahedral intermediate formation is the rate-limiting step of the acylation process and the whole reaction. This species evolves to produce the acyl-enzyme product. However, the AM1/MM reaction barrier was highly overestimated when a comparison with experimental kinetics data was done.[12,31]

In this work, the quantum-corrected free energy profile (which includes quantized vibrational energies) for the acylation reaction has been characterized at the SCC-DFTB/CHARMM22 theoretical level within the framework of the EA-VTST(MT) theory. There is no evidence for the formation of the stable tetrahedral intermediate obtained in the previous theoretical studies or in other serine proteases. The acylation reaction is concluded to proceed through a concerted mechanism that involves a single transition state (TS2) in which the tetrahedral geometry has already been adopted and the peptide bond is starting to break. The free energy necessary to reach TS2 from the reactants is the kinetically relevant (rate-limiting) barrier for the acylation process.

Our best theoretical estimation of the free energy barrier for this acylation step is $\Delta G^{\ddagger}_{phen}(T)$ = 21.0 kcal/mol, in qualitative agreement with the experimentally derived value of 18.7 kcal/mol. A calculated KIE of 2.0 has also been predicted, indicating that the H^+ transfer is 2 times faster than the D^+ transfer. This difference mainly arises from the higher free energy barrier in the case of the D^+ transfer, since the tunneling (1.19 and 1.14 for H^+ and D^+, respectively) and recrossing factors (0.38 and 0.47 for H^+ and D^+, respectively) are similar for both isotopic substitutions.

We hope that this information can be of help in the development of new NS3/NS4A inhibitors based on transition state analogues, for which the characterized TS2 structure can be a good starting point.

■ ASSOCIATED CONTENT

Supporting Information

The following file is available free of charge on the ACS Publications website at DOI: 10.1021/cs5011162.

Fragments of the NS5A/5B substrate and residues of the NS3 protease included in the QM region (Figure S1), fitting of polynomial coefficients and ΔW_{vib} values for the nucleophilic attack and peptide bond breaking steps (Table S1 and Figure S2), minimum energy profiles (Figure S3) and parts of the potential energy surface (Figure S4) corresponding to the nucleophilic attack and

dx.doi.org/10.1021/cs5011162 | ACS Catal. 2015, 5, 246−255

peptide bond breaking steps, structure and potential energy of the stationary points (Figures S5 and S6 and Table S2), and AIM analysis (Table S3) (PDF)

AUTHOR INFORMATION

Corresponding Authors

*E-mail for M.G.: miguel.gonzalez@ub.edu.
*E-mail for L.M.: laura.masgrau@uab.cat.
*E-mail for R.M.: rodrigo.martinez@unirioja.es.

Notes

The authors declare no competing financial interest.

ACKNOWLEDGMENTS

This work was supported by the Spanish Ministry of Science and Innovation (MICINN projects CTQ2011-27857-C02-01 and CTQ2011-24292). Thanks are also given to the University of La Rioja (project API 09/14) and the "Generalitat de Catalunya" (Autonomous Government of Catalonia, reference nos. 2009SGR17, 2009SGR409, and XRQTC). JA.M.-G. acknowledges the Autonomous Government of La Rioja for a predoctoral research grant. L.M. also thanks the "Programa UAB-Banco Santander". Finally, the authors thank Dr. Mireia García-Viloca for her helpful comments.

REFERENCES

(1) World Health Organization, Global Alert and Response (GAR), Hepatitis C. http://www.who.int/csr (accessed: July 28, 2014).
(2) Perz, J. F.; Armstrong, G. L.; Farrington, L. A.; Hutin, Y. J.; Bell, B. P. *J. Hepatol.* **2006**, *45*, 529−938.
(3) Feeney, E. R.; Chung, R. T. *The BMJ* **2014**, *349*, g3308 DOI: 10.1136/bmj.g3308.
(4) Tan, S.-L. *Hepatitis C Viruses: Genomes and Molecular Biology*; Horizon Bioscience: Norfolk, VA, 2006.
(5) Liang, T. J.; Ghany, M. G. *N. Engl. J. Med.* **2013**, *368*, 1907−1917.
(6) Liverton, N. J.; Holloway, M. K.; McCauley, J. A.; Rudd, M. T.; Butcher, J. W.; Carroll, S. S.; DiMuzio, J.; Fandozzi, C.; Gilbert, K. F.; Mao, S. S.; McIntyre, C. J.; Nguyen, K. T.; Romano, J. J.; Stahlhut, M.; Wan, B. L.; Olsen, D. B.; Vacca, J. P. *J. Am. Chem. Soc.* **2008**, *130*, 4607−4609.
(7) Love, R. A.; Parge, H. E.; Wickersham, J. A.; Hostomsky, Z.; Habuka, N.; Moomaw, E. W.; Adachi, T.; Hostomska, Z. *Cell* **1996**, *87*, 331−342.
(8) Kwong, A. D.; Kim, J. L.; Rao, G.; Lipovsek, D.; Raybuck, S. A. *Antiviral Res.* **1998**, *40*, 1−18.
(9) Barbato, G.; Cicero, D. O.; Cordier, F.; Narjes, F.; Gerlach, B.; Sambucini, S.; Grzesiek, S.; Matassa, V. G.; De Francesco, R.; Bazzo, R. *EMBO J.* **2000**, *19*, 1195−1206.
(10) Fersht, A. R.; Sperling, J. *J. Mol. Biol.* **1973**, *74*, 137−149.
(11) Hedstrom, L. *Chem. Rev.* **2002**, *102*, 4501−4523.
(12) Rodríguez, A.; Oliva, C.; González, M. *Phys. Chem. Chem. Phys.* **2010**, *12*, 8001−8015.
(13) Colarusso, S.; Koch, U.; Gerlach, B.; Steinkühler, C.; De Francesco, R.; Altamura, S.; Matassa, V. G.; Narjes, F. *J. Med. Chem.* **2003**, *46*, 345−348.
(14) Han, W.; Hu, Z.; Jiang, X.; Wasserman, Z. R.; Decicco, C. P. *Bioorg. Med. Chem. Lett.* **2003**, *13*, 1111−1114.
(15) Grakoui, A.; McCourt, D. W.; Wychowski, C.; Feinstone, S. M.; Rice, C. M. *J. Virol.* **1993**, *67*, 2832−2843.
(16) Zhang, R.; Durkin, J.; Windsor, W. T.; McNemar, C.; Ramanathan, L.; Le, H. V. *J. Virol.* **1997**, *71*, 6208−6213.
(17) Urbani, A.; Bianchi, E.; Narjes, F.; Tramontano, A.; De Francesco, R.; Steinkühler, C.; Pessi, A. *J. Biol. Chem.* **1997**, *272*, 9204−9209.
(18) Dimasi, N.; Pasquo, A.; Martin, F.; Di Marco, S.; Steinkühler, C.; Cortese, R.; Sollazzo, M. *Protein Eng.* **1998**, *11*, 1257−1265.
(19) Steinkühler, C.; Biasiol, G.; Brunetti, M.; Urbani, A.; Koch, U.; Cortese, R.; Pessi, A.; De Francesco, R. *Biochem.* **1998**, *37*, 8899−8905.
(20) Koch, U.; Biasiol, G.; Brunetti, M.; Fattori, D.; Pallaoro, M.; Steinkühler, C. *Biochem.* **2001**, *40*, 631−640.
(21) Beyer, B. M.; Zhang, R.; Hong, Z.; Madison, V.; Malcolm, B. A. *Proteins: Struct. Funct. Bioinf.* **2001**, *43*, 82−88.
(22) Thibeault, D.; Bousquet, C.; Gingras, R.; Lagacé, L.; Maurice, R.; White, R. W.; Lamarre, D. *J. Virol.* **2004**, *78*, 7352−7359.
(23) Geitmann, M.; Dahl, G.; Danielson, U. H. *J. Mol. Recognit.* **2011**, *24*, 60−70.
(24) Lemke, C. T.; Goudreau, N.; Zhaho, S. P.; Hucke, O.; Thiveault, D.; Llinas-Brunet, M.; White, P. W. *J. Biol. Chem.* **2011**, *286*, 11433−11443.
(25) Topf, M.; Varnai, P.; Richards, W. G. *J. Am. Chem. Soc.* **2002**, *124*, 14780−14788.
(26) Ishida, T.; Kato, S. *J. Am. Chem. Soc.* **2003**, *125*, 12035−12048.
(27) Ishida, T.; Kato, S. *J. Am. Chem. Soc.* **2004**, *126*, 7111−7118.
(28) Shokhen, M.; Albeck, A. *Proteins: Struct. Funct. Bioinf.* **2004**, *54*, 468−477.
(29) Ishida, T. *Biochem.* **2006**, *45*, 5413−5420.
(30) Zhou, Y.; Zhang, Y. *Chem. Commun.* **2011**, *47*, 1577−1579.
(31) Oliva, C.; Rodríguez, A.; González, M.; Yang, Y. *Proteins: Struct. Funct. Bioinf.* **2007**, *66*, 444−455.
(32) Rodríguez, A.; Oliva, C.; González, M.; van der Kamp, M.; Mulholland, A. J. *J. Phys. Chem. B* **2007**, *111*, 12909−12915.
(33) Martínez, J. A. QM/MM study of the mechanism and kinetics of the reactions of the Hepatitis C virus NS3 protease with its main substrates. Ph.D. Thesis, University of La Rioja, September, 2013.
(34) Cui, Q.; Elstner, M.; Kaxiras, E.; Frauenheim, T.; Karplus, M. *J. Phys. Chem. B* **2001**, *105*, 569−585.
(35) García-Viloca, M.; Alhambra, C.; Truhlar, D. G.; Gao, J. *J. Chem. Phys.* **2001**, *114*, 9953−9958.
(36) Alhambra, C.; Corchado, J.; Sánchez, M. L.; García-Viloca, M.; Gao, J.; Truhlar, D. G. *J. Chem. Phys. B* **2001**, *105*, 11326−11340.
(37) Truhlar, D. G.; Gao, J.; García-Viloca, M.; Alhambra, C.; Corchado, J.; Sánchez, M. L.; Poulsen, T. D. *Int. J. Quantum Chem.* **2004**, *100*, 1136−1152.
(38) Masgrau, L.; Truhlar, D. G. *Acc. Chem. Res.* **2014**, DOI: 10.1021/ar500319e.
(39) Elstner, M.; Porezag, D.; Jungnickel, G.; Elsner, J.; Haugk, M.; Frauenheim, T.; Suhai, S.; Seifert, G. *Phys. Rev. B* **1998**, *58*, 7260−7268.
(40) Elstner, M. *Theor. Chem. Acc.* **2006**, *116*, 316−325.
(41) MacKerell, A. D., Jr.; Bashford, D.; Bellott, M.; Dunbrack, R. L., Jr.; Evanseck, J. D.; Field, M. J.; Fischer, S.; Gao, J.; Guo, H.; Ha, S.; Joseph-McCarthy, D.; Kuchnir, L.; Kuczera, K.; Lau, F. T. K.; Mattos, C.; Michnick, S.; Ngo, T.; Nguyen, D. T.; Prodhom, B.; Reiher, W. E.; Roux, B.; Schlenkrich, M.; Smith, J. C.; Stote, R.; Straub, J.; Watanabe, M.; Wiórkiewicz-Kuczera, J.; Yin, D.; Karplus, M. *J. Phys. Chem. B* **1998**, *102*, 3586−3616.
(42) Brooks, B. R.; Brooks, C. L., III; Mackerell, A. D.; Nilsson, L.; Petrella, R. J.; Roux, B.; Won, Y.; Archontis, G.; Bartels, C.; Boresch, S.; Caflisch, A.; Caves, L.; Cui, Q.; Dinner, A. R.; Feig, M.; Fischer, S.; Gao, J.; Hodoscek, M.; Im, W.; Kuczera, K.; Lazaridis, T.; Ma, J.; Ovchinnikov, V.; Paci, E.; Pastor, R. W.; Post, C. B.; Pu, J. Z.; Schaefer, M.; Tidor, B.; Venable, R. M.; Woodcock, H. L.; Wu, X.; Yang, W.; York, D. M.; Karplus, M. *J. Comput. Chem.* **2009**, *30*, 1545−1615.
(43) Field, M. J.; Bash, P. A.; Karplus, M. *J. Comput. Chem.* **1990**, *11*, 700−733.
(44) Hou, G.; Cui, Q. *J. Am. Chem. Soc.* **2013**, *135*, 10457−10469.
(45) Zhang, Z.; Shanshan, W.; Dingguo, X. *J. Phys. Chem. B* **2013**, *117*, 6635−6645.
(46) Gao, J.; Amara, P.; Alhambra, C.; Field, M. J. *Mol. Phys.* **2003**, *101*, 2695−2714.
(47) Pu, J.; Gao, J.; Truhlar, D. G. *J. Phys. Chem. A* **2004**, *108*, 5454−5463.
(48) Chu, J. W.; Trout, B. L.; Brooks, B. R. *J. Chem. Phys.* **2003**, *119*, 12708−12717.

(49) Brooks, C. L., III; Karplus, M. *J. Chem. Phys.* **1983**, *79*, 6312−6325.
(50) Ryckaert, J. P.; Ciccotti, G.; Berendsen, H. J. C. *J. Comput. Phys.* **1977**, *23*, 327−341.
(51) Kästner, J. *WIRES Comp. Mol. Scien.* **2011**, *1*, 932−942.
(52) Kumar, S.; Bouzida, D.; Swendsen, R. H.; Kollman, P. A.; Rosenberg, J. M. *J. Comput. Chem.* **1992**, *13*, 1011−1021.
(53) Grossfield, A. *WHAM: an implementation of the weighted histogram analysis method v 2.06*; http://membrane.urmc.rochester.edu/content/wham/ (accessed: July 28 2014).
(54) Luk, L. Y. P.; Ruiz-Pernía, J. J.; Dawson, W. M.; Roca, M.; Loveridge, E. J.; Glowacki, D. R.; Havey, J. N.; Mulholland, A. J.; Tuñon, I.; Moliner, V.; Allemann, R. K. *Proc. Natl. Acad. Sci. U.S.A.* **2013**, *110*, 16344−16349.
(55) Truhlar, D. G.; Isaacson, A. D.; Garret, B. C. Generalized Transition State Theory. In *Theory of Chemical Reaction Dynamics*; Baer, M., Ed.; CRC Press: Boca Raton, FL, 1985; Vol. *4*, p 65.
(56) Liu, Y.-P.; Lu, D.-H; González-Lafont, A.; Truhlar, D. G.; Garret, B. C. *J. Am. Chem. Soc.* **1993**, *115*, 7806−7817.
(57) Garcia-Viloca, M.; Alhambra, C.; Corchado, J. C.; Sanchez, M. L.; Villa, J.; Gao, J.; Truhlar, D. G. *CHARMMRATE-version 2.0*; University of Minnesota, Minneapolis, MN, 2002.
(58) Corchado, J. C.; Chuang, Y.-Y.; Fast, P. L.; Villa, J.; Hu, W.-P.; Liu, Y.-P.; Lynch, G. C.; Nguyen, K. A.; Jackels, C. F.; Melissas, V. S.; Lynch, B. J.; Rossi, I.; Coitino, E. L.; Fernandez-Ramos, A.; Pu, J.; Albu, T. V.; Steckler, R.; Garrett, B. C.; Isaacson, A. D.; Truhlar, D. G. *POLYRATE-version 9.0*; University of Minnesota, Minneapolis, MN, 2002.
(59) Garcia-Viloca, M.; Truhlar, D. G.; Gao, J. *Biochem.* **2003**, *42*, 13558−13575.
(60) Frushicheva, M.-P.; Warshel, A. *ChemBioChem* **2012**, *13*, 215−223.
(61) Yennawar, N. H.; Yennawar, H. P.; Farber, G. K. *Biochemistry* **1994**, *33*, 7326−7326.
(62) Liu, B.; Schofield, C. J.; Wilmouth, R. C. *J. Biol. Chem.* **2006**, *281*, 24024−24035.
(63) Romano, K. P.; Ali, A.; Aydin, C.; Soumana, D.; Ozen, A.; Deveau, L. M.; Silver, C.; Cao, H.; Newton, A.; Petropoulos, C. J.; Huang, W.; Schiffer, C. A. *PLOS Pathog.* **2012**, *8*, e1002832.
(64) Świderek, K.; Martí, S.; Moliner, V. *ACS Catal.* **2013**, *4*, 426−434.
(65) Jencks, W. P. *Chem. Soc. Rev.* **1981**, *10*, 345−375.
(66) Schramm, V. L. *Annu. Rev. Biochem.* **1998**, *67*, 693−720.
(67) Schramm, V. L. *Annu. Rev. Biochem.* **2011**, *80*, 703−732.
(68) Di Marco, S.; Rizzi, M.; Volpari, C.; Walsh, M. A.; Narjes, F.; Colarusso, S.; De Francesco, R.; Matassa, V. G.; Sollazzo, M. *J. Biol. Chem.* **2000**, *275*, 7152−7157.
(69) Lin, C.; Kwong, A. D.; Perni, R. B. *Infectious Disorders-Drug Targets* **2006**, *6*, 3−15.